
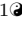
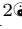

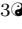



# Sizing of airborne particles in an operating room


Peter T. Tkacik<sup>1\*</sup>, Jerry L. Dahlberg<sup>1</sup>, James E. Johnson<sup>2</sup>, James J. Hoth<sup>2</sup>,  
Rebecca Szer<sup>3</sup>, Samuel Hellman<sup>4</sup>

**1** Department of Mechanical Engineering, University of North Carolina at Charlotte, Charlotte, North Carolina, USA

**2** Department of General Surgery, Wake Forest School of Medicine, Winston-Salem, North Carolina, USA

**3** Organized Healthcare Education, Garnet Health Medical Center, Middleton, New York, USA

**4** Department of Medical Physics, Memorial Sloan Kettering Cancer Center, New York, New York, USA

 These authors contributed equally to this work.

\* ptkacik@uncc.edu

## Abstract

Medical procedures that produce aerosolized particles are under great scrutiny due to the recent concerns surrounding the COVID-19 virus and increased risk for nosocomial infections. For example, thoracostomies, tracheotomies and intubations/extubations produce aerosols that can linger in the air. The lingering time is dependent on particle size where, e.g., 500  $\mu\text{m}$  (0.5 mm) particles may quickly fall to the floor, while 1  $\mu\text{m}$  particles may float for extended lengths of time [1–6].

Here, a method is presented to characterize the size of 25  $\mu\text{m}$  to 400  $\mu\text{m}$  particles resulting from surgery in an operating room (OR). The particles are measured in situ (next to a patient on an operating table) through an aperture in a 400 mm rectangular enclosure. The technique employs principles of some existing ex situ optical particle counters, however, it allows less flow restriction and provides measurements across a larger field of view (FOV). The particles and gasses exiting a patient are vented through an enclosed laser sheet while a camera captures images of the side-scattered light from the entrained particles. A similar optical configuration was described by Anfinrud *et al.* [7]; however, we present here an extended method which provides a calibration method for determining particle size.

The use of a laser sheet with side-scattered light provides a large FOV and bright image of the particles; however, the particle image dilation caused by scattering does not allow direct measurement of particle size. The calibration routine presented here is accomplished by measuring fixed particle distribution ranges with a calibrated shadow imaging system and mapping these measurements to the in-situ imaging system.

## Introduction

In the same way that modifications were made to protocols related to blood borne pathogens at the onset of the AIDS crisis, medical procedures that produce aerosolized particles are under great scrutiny due to the recent concerns surrounding the spread of COVID-19 [8]. Aerosols from chest tube insertion (thoracostomies) and throat tube insertion (tracheotomies), which can range in size from 500  $\mu\text{m}$  particles (which may

quickly fall to the floor) down to 1  $\mu\text{m}$  particles (which may float for extended lengths of time), are of interest to surgeons and emergency health personnel. The differences in particle size and quantity expelled during these and other types of procedures affect the potential viral load in the air.

Here, we present a method to measure the size of entrained, microscopic fluid particles expelled from a patient during aerosol-generating procedures (AGP). Because the particles are small (high image resolution desired) and the region of interest (ROI) is large (reduced resolution given the same number of pixels), there is an inherent challenge in deploying an imaging solution to cover this large dynamic range. The procedure developed for this paper is an extension of a method used by Anfinrud *et al.* [7] which describes a technique but not the calibration method or limitations.

This technique allows quantitative characterization of the size of these particles. The result is a two-part process where 1) particles in a range of sizes are produced and measured using a calibrated, high-resolution shadow method and 2) the same particle generators are measured with the *in-situ*, laser-based shadow imaging system and a correlation mapping is made between the (dilated) laser image size and the measured particle size.

## Materials and methods

### Calibration: Generation and measurement of particles using shadow imaging method

The aerosol particles being studied present two issues with regards to optical measurements; first, they are microscopic, (ranging from  $< 30 \mu\text{m}$  to  $> 500 \mu\text{m}$ ) and second, they are moving quickly, (up to 10 m/s). Particle size measurements using shadow imaging (back lighting) can be a reliable method which allows for linear calibration/scaling of particle images as well as the measurement of particle velocity; however, the size and speed of the particles during some AGP required the use of a high-speed camera [9] with high-magnification optics and laser illumination (described below). The laser-based imaging technique used *in situ* is not able to be linearly scaled due to image dilation inherent in side-scattering. Thus, a method of calibrating the laser-based system using a shadow imaging system was developed.

### Particle generators

As shown in Fig 1, modified spray bottle nozzles were used to produce a range of particle size distributions. Using a vibrating orifice generator would also work well and give a single monodisperse size [10,11], however, the spray bottle solution was chosen due to low cost, flexibility and easy reproducibility. Five particle size ranges were created using nozzles with varying orifice diameters. The standard orifice size of the nozzles was modified by drilling, and the following diameters were used: 0.30 mm, 0.46 mm, 0.56 mm, 0.74 mm, and 1.00 mm. These produced particles with distribution ranges centered between  $\sim 20 \mu\text{m}$  and  $\sim 650 \mu\text{m}$ .

### Fig 1. Particle Generator with several of the modified nozzles

While several fluids were tested, water was ultimately chosen due to its minimal environmental concerns and because it most closely matches the luminance of bodily fluids expelled during AGP.

## Spatial and temporal resolution requirements

In order to image small particles with a linearly-scaled measurement system, sufficiently high spatial resolution is needed such that each imaged particle occupies more than one pixel. In the shadow imaging (calibration) configuration, one pixel in the object plane represents 20.1  $\mu\text{m}$  in the image plane. To enable this macro focus configuration, a 35 mm lens [12] was used along with a 6.8 mm extension ring. The focus was set at minimum distance and a scaled calibration target (ruler) was positioned in the focal plane ( $\sim 70$  mm from the lens). The aperture was set to the lens minimum of  $f/2.8$

In order to acquire enough particle images during each spray event (duration of 0.08 s), an acquisition speed of 10,000 frames per second (fps) was chosen. Due to bandwidth limitations of the camera at 10,000 fps, a cropped ROI of 388 x 344 pixels was used. The spatial resolution of 20.1  $\mu\text{m}$  corresponded with an image plane which was 7.9 mm horizontally and 7.11 mm vertically. At the chosen frame rate and macro scale, the high velocity of the particles required an exposure time of 23  $\mu\text{s}$  to avoid particle streaking in the image.

## Calibration test protocol for high-speed shadow imaging measurements

The exposure time of 23  $\mu\text{s}$  required the use of a high-intensity light source [13,14]. When this lamp is set at maximum power and shining directly into the camera lens from less than a meter away (see Fig 2), the imaging sensor can easily become overheated. In order to prevent sensor damage, we used a test protocol as follows:

**Fig 2. Experimental Set up containing A) high-intensity light, B) particle generator and C) high speed camera.**

1. Set the camera to record in loop mode onto circular buffer (6 s loop time).
2. Quickly rotate the lamp onto the FOV.
3. Send pre trigger to the camera to start recorded loop.
4. Generate the particles, spraying them across the FOV. Duration of approximately 0.08 s.
5. Immediately turn the lamp away from the camera—typically less than the full six seconds of exposures were acquired.

## Calibration FOV

For the calibration imaging configuration, the FOV was approximately 7.9 x 7.1 mm in the image plane (Fig 3). To position the setup repeatably, a metal frame was constructed that supported the camera, spray nozzle and a translating fixture to position the calibration ruler— 6 in (152.4 mm) x 3/16 in (4.76 mm) with 1/64 in (0.4 mm) resolution [15] - in the FOV. The rigidity of the frame allowed for fine adjustment of focus which could subsequently be locked on the lens.

**Fig 3. Experimental set up showing A) camera lens, B) insertion reference line on particle shield, C) 3 mm aperture in particle shield, D) 7.9 x 7.1 mm field of view and E) steel ruler.**

Due to the small FOV, it was easy to lose track of the image plane position in space. To address this issue, the ruler was positioned such that, after calibration images were

acquired, it could be accurately shifted in the image plane with a small portion remaining visible in the FOV during recording. The dark edge in the upper right corner of the images (e.g. Fig 4) is the tip of the ruler. The ruler also assisted by providing a reference location towards which the particles could be sprayed during testing.

**Fig 4. Example image of the particles from 0.74 mm nozzle; 10,000 fps, 23  $\mu$ s exposure**

### Calibration depth of field (DOF)

Due to the large aperture of the lens (f/2.8) required for acquisition with a relatively short exposure time, the resulting DOF was only a few millimeters which could result in imaging many particles outside of the focal plane. In order to reduce the number of out-of-focus particles, a shield was used to limit the location of the particles to this shallow DOF. The shield (Figs 3 and 5) was made from a  $\varnothing$ 50 mm ( $\varnothing$  = diameter) x 70 mm long plastic cylinder with one end open and the other restricted by a  $\varnothing$ 3 mm orifice. The particles were sprayed into the shield and only exited through the  $\varnothing$ 3 mm aperture on the far end. The cylinder was painted flat black to minimize laser reflections.

**Fig 5. Experimental set up including A) Particle Shield, B) Particle Shield, B) 0.012" Particle Generator, C) Particle Shield Aluminum Bracket and D) High-Speed Camera**

An aluminum bracket was fabricated to hold and align the particle generators (sprayers) with the shield and the bracket was mounted to the calibration frame. A silver reference line was drawn around the circumference as a visual aid for repeatable insertion depth into the OR system as seen in Figs 3 and 5.

### Calibrated particle size measurement

The high-speed camera [9] images were acquired using the manufacturer's supplied image capture software [16]. This system acquires the high-speed images as a collection of single TIFF format frames. Each calibration test resulted in 6,000 recorded frames, of which only those with particles visible in the FOV were stored (between 80 to 120 frames per experiment). These image sets were acquired in technical replicates for each of the five orifice sizes, (0.30, 0.46, 0.56, 0.74, and 1.0 mm). Fig 4 shows an example of a single image gathered during one of the tests with a 0.74 mm orifice.

The same software was also used to play back the sequences where each particle size, position, and velocity were manually measured. Particle velocity was determined by tracking the position across successive frames while size was determined by measuring the particle diameter in the image (in pixels) and multiplying by the 20.1  $\mu$ m/pixel scale factor. The standard deviation of the velocity was used as a data recording check, (i.e., the range of standard deviation was about 0.15 to 0.20 and an input error would typically result in a value over 100).

### Out-of-focus particles

While the previously described shield limited the number of out-of-focus particles, there were still some captured in the calibration images. To minimize the error of diameter measurement due to blurry particles, two methods were employed. First, only reasonably clear particles (qualitatively assessed) were measured.

Secondly, a diameter estimation technique was developed with a calculation made to determine the effective diameter of a marginally blurry particle. An ROI of

approximately twice the estimated particle size was selected around each particle to be analyzed, (e.g., 16 x 19 pixels for a 10.4 pixel diameter particle and 8 x 10 for a 4.3 pixel diameter particle). The gray values were normalized by the average background (bright) value and the pixels were then inverted such that each pixel is calculated by using Eq 1,

$$G_e = \left(\frac{G}{G_b}\right)^{-1} \quad (1)$$

where  $G_e$  is the effective pixel gray value,  $G$  is the captured gray value and  $G_b$  is the average background gray value. For an ideal shadow image with perfect focus/contrast, this would result in a gray value of 1 for all pixels inside the imaged particle and 0 for all background pixels. In actual captured images—and particularly for blurred images—a gradient is present. The calculated diameter was determined by summing all resulting gray values in the ROI and treating this sum as the effective particle area [in pixels]. From this effective area, the diameter was calculated assuming a circular particle with Eq 2,

$$A_e = \frac{\pi * d_e^2}{4} \quad (2)$$

where  $A_e$  is the effective area and  $d_e$  is the effective diameter. Thus, the effective diameter [in pixels] was calculated using Eq 3,

$$d_e = \sqrt{\frac{A_e}{4 * \pi}} \quad (3)$$

and converted to  $\mu\text{m}$  using the scale factor of 20.1  $\mu\text{m}/\text{pixel}$ .

Qualitatively assessing the edge determination on several examples indicated that the calculated diameter of a marginally out-of-focus particle was a good representation of the physical boundary. The calculated edge was approximately halfway through the perimeter gradient of the imaged spot; midway between the dark central shadow and the bright background level.

### Results of high-speed measurements

In total, 260 particles were measured. Each nozzle was tested in technical replicates and within each experimental run, every particle was measured multiple times (average 5 times) in successive image frames as it traversed across the FOV. Measurements from all five particle generators—including replicates—were combined for subsequent analysis. Fig 6 shows the distribution of measured particles.

**Fig 6. Histogram of particles counts in high speed shadow method by size.**

### In-situ measurements with OR system: laser-based imaging in mobile enclosure

The generation and measurement of particles using the shadow imaging method described in the calibration section yielded the reference data needed for calibration of the in-situ, OR measurement system (“OR System”). For measurements in an OR environment, a mobile system was developed with a non-intrusive FOV ten times larger ( $\sim 75$  mm square versus  $\sim 7.9$  mm square) than the calibration configuration. The

mobile system can be moved easily to the OR and the combined system weight for the aluminum frame, enclosure, camera, laser, etc. is 14 kg. The OR System includes a dark enclosure designed to allow recording of the side-scattered laser light from particles produced by the same particle generators detailed in the previous calibration section. Repeating measurements on the same particle generators with both systems allowed us to correlate the imaged particles diameters from scattered laser light in the OR System to the particle sizes measured in the calibration system.

### Aluminum support frame

For the OR environment, the two most critical concerns are safety (for health care practitioners and patients) and repeatable placement of the test equipment. Both concerns are primarily related to the control and positioning of the laser system. The laser must be a) in a fixed position with its beam and reflections contained and b) rigidly aligned with respect to the camera. To this end, an adjustable aluminum frame was fabricated to support the entire system. The frame is symmetric such that the laser and camera can be reversed to allow work on either side of the patient [17].

### Light containment enclosure

The OR System as seen in Figs 7-9 includes a dark enclosure which contains the particle flow from the patient along with the laser light and reflections. There are apertures for the particles exiting the patient as well as to allow access for the camera and laser. It is constructed of black foam board (6 mm thick) and has outer dimensions of 457 x 457 x 305 mm with a volume of 63.7 liters; smaller enclosures were found to cause flow restrictions. To minimize weight, the aluminum frame supports the enclosure at its lower outside corners and foam board structure is held in place with an elastic rubber cord. This allows the break-down for transport, quick access to the inside and simple replacement. Since the frame does not fully surround the enclosure, this also allows simple and flexible modification for different surgical procedures, anatomical locations and levels of access; the foam board can be easily cut with a craft knife (e.g., X-Acto) prior to surgery to increase access. In the most extreme case, the whole front and much of the bottom could be cut away.

**Fig 7. . OR system with laser in left side orientation and circular intake aperture.**

**Fig 8. Rear of enclosure showing tablet with support frame, fan, and laser beam trap boxes.**

**Fig 9. Schematic of OR system in left thoracotomy/thoracostomy orientation.**

While the authors created a flexible system design which can accommodate many procedures, the enclosure in the present study was configured for lateral thoracic access (required for, e.g., thoracotomy/thoracostomy). In this configuration, the enclosure box sits on the patient's side and is fit as close as possible to the axilla with its long edge roughly parallel to the abdomen. There are two apertures directly opposite one another on the lateral sides of the enclosure close to the proximal (superior) end (near the axilla). One aperture (entrance aperture) is positioned around the incision site to allow particles from the patient to enter the enclosure, while the opposite aperture (camera

aperture) allows the camera to view the particles. The camera looks directly across the enclosure at the entrance aperture. Laser light enters through a slit in the distal (inferior) end of the enclosure normal to the viewing axis of the camera. The entrance aperture has a light "friction-fit" removeable ring which allows it to be changed from  $\varnothing 75$  mm to  $\varnothing 120$  mm, although most measurements were made with the  $\varnothing 75$  mm ring.

### Laser beam traps

In order to minimize laser reflections, black cardboard beam trap boxes are attached to the enclosure and held in place by diagonal braces (see Fig 7). These boxes are 150 mm tall and have a 15 mm wide vertical entrance slit. There are two boxes to allow use for configurations with the laser on either side. After the slit, an internal diagonal board reflects the light sideways into a chamber which has a narrow converging section. Despite the intensity of the laser light, these beam trap boxes minimized reflected light well and, even during a 45-minute trial, did not overheat.

### Filtered air

A 100 mm (Fig 10) square fan with air filter is installed on the upper left side of the enclosure to maintain positive pressure with clean air and minimize noise in the data from airborne dust. It is used in the OR but needs to be turned off during experiments as it is powerful enough to reduce particle flow into the enclosure. It is constructed from a common brushless DC motor (a.k.a. "muffin") fan, blows into the enclosure through a HEPA air filter, and is powered by a 12 VDC battery.

**Fig 10. Entrance aperture and filter fan on side of enclosure.**

### Camera

The experiments were recorded with a computer tablet [18] set to acquire video in 4K-60 mode to achieve video with a resolution of 3840 x 2160 pixels at 60 fps. The tablet is mounted in a removeable (left or right side) support frame against the camera aperture located directly across from the entrance aperture of the enclosure. As described in the light containment enclosure section, the camera views across the enclosure directly into the entrance aperture to record particles coming from either the particle generator or patient exhaust gas.

To focus the camera on the desired FOV, a 20 mm square micro-detailed focus target was clipped to the entrance aperture and positioned in the plane of the laser sheet. A flashlight was then directed onto the target from the camera aperture. With the target illuminated, the image of the focus target was pressed until the tablet focused on the target. Once focused on the target, both the focus and the exposure were locked (AEAF Lock).

### OR System Test Measurements

In order to map the particle diameter measurements from the shadow imaging calibration data, the same particle generators were measured in the enclosure of the OR System. The particle generators and nozzles described in the particle generators section (including shield) were measured in the OR System. To acquire the test video, the following procedure was followed.

1. Turn on the laser and let it warm up to full power.

- 2. Run the air filter fan for at least 30 seconds. 235
- 3. Insert focus target. 236
- 4. Illuminate focus target. 237
- 5. Focus camera and lock the camera settings. 238
- 6. Remove focus target. 239
- 7. Turn off fan. 240
- 8. Start recording video. 241
- 9. Insert and spray the particle generator several times. 242
- 10. Stop recording 243

Each video was converted to a string of single TIFF images (sample image shown in Fig 11). From the five particle generator nozzles (with technical replicates for each size), 1123 particles were measured. For the OR System, the camera frame rate is lower and, thus, most particles were only measured once during each experiment since they did not generally appear in more than one frame of the video. In several cases, repeat measurements were possible, however, transverse velocity data was not used due to this limitation. The effective diameters of the particles were determined using the same technique described in the calibrated particle size measurement and out-of-focus particles sections, without the last step of converting from pixels to physical units. This resulted in an effective diameter [in pixels] for each particle measured.

**Fig 11. Single image frame from video of 0.46 mm particle generator experiment showing scattered laser light from particles.**

**Correlation of Mobile OR System and Calibration Measurements**

Since the same particle generators were used along with the same number of repeat measurements for each size, it is assumed that the distribution of particle sizes should be similar between the shadow imaging calibration data and the data measured in the OR System. However, the total number/magnitude of measured particle counts did not match between the two systems due to a) large difference in field of view and b) differences in system sensitivity. In order correlate the two histograms’ distributions, the OR System test measurement data counts were normalized to the calibration data using a constant scale factor. The two distributions were then parsed into varying numbers of bins in order to converge on a best fit to the calibration data. Additionally, overflow and underflow bins were used due to linear resolution limits of the OR System (all particles above and below the linear resolution limits appear to be the same sizes in a scattered-light configuration).

The best fit result was a ten-bin parsing of the ranges (as seen in Fig 12, a maximum range (overflow bin) collecting all particles above 600 microns, and a minimum range (underflow bin) collecting all particles less than 45 microns.

The resulting data fit yielded a correlation mapping between the effective diameters measured with the OR System and the calibrated diameters measured with shadow imaging setup such that

$$d(B) = 15.374 * B - 168.7 \tag{4}$$



where  $d$  is the particle diameter in microns and  $B$  is the measured effective diameter in pixels. 273  
274

Due to the previously mentioned linear resolution limits, this relationship fails below a measured effective diameter of 13.9 pixels and thus a linear fit to zero was used below this point. The final conversion function was 275  
276  
277

$$d(B) = \begin{cases} 15.374 * B - 168.7, B > 13.9 \\ 3.2374 * B, B \leq 13.9 \end{cases} \quad (5)$$

It should be noted that this correlation function is highly dependent on the systems and equipment being used. This includes the cameras, lenses, recording mode and resolution, laser and power level, optical setup etc. This calibration procedure can be used with a wide variety of equipment to yield specific and repeatable calibration values. 278  
279  
280  
281

**Fig 12. Histogram of particles parsed into ten ranges for improved match.**

## Results and Discussion 282

One of the benefits of the described method is that it is adaptable to many other AGP measurements. This flexibility is a result of the non-contact approach to measurement; that is, the flow across a large aperture can be measured in situ as opposed to diverting (and thus modifying) the flow into a pipe or other passage. 283  
284  
285  
286

Laser side-scatter imaging increases the possible FOV size and thus offers the ability to measure particles below the linear resolution of the camera. That is, even if the particles are smaller than the pixel resolution of the camera's sensor, the scattered laser light can amplify their effective image size. This method provides a correlation between the imaged side-scatter particle diameters and their physical size. 287  
288  
289  
290  
291

The authors employed inexpensive and readily available components that were easily accessible and likely to exist in many research institutions and hospitals. As an example, superior high-resolution, high-speed cameras are available; however, most contemporary tablets available today have an amazing ability to capture video at high resolution and proved to be sufficient for this application. 292  
293  
294  
295  
296

There are several areas where this method could be improved for long term use. The first of which is the use of commercially available software packages that could automate the particle size measurement. This would remove some of the potential errors associated with the manual processing and improve the ability to perform measurement error analysis. Additionally, a more appropriate, scientific camera could remove potential variability due to the tablet's limited lens control and automatic image compression. In combination with the camera and software, an improved method of generating particles with more controlled sizes—such as with a vibrating orifice generator—would improve the precision of resulting calibration. 297  
298  
299  
300  
301  
302  
303  
304  
305

Finally, improving the design to make a modular or compressed enclosure/laser to allow a better fit to a patient which could be supported from an overhead arm as used in ORs would make the system more user-friendly. 306  
307  
308

## Summary 309

We present a system for in situ measurement of airborne particles in a large field of view and include a calibration method for quantifying particle size. The calibration method, equipment and system design—which allows for use in specialized AGPs—is described. 310  
311  
312

The optical measurement system (OR System) uses a laser side-scatter technique to yield measurements of airborne particles in the range of less than 25  $\mu\text{m}$  to over 600  $\mu\text{m}$  across a relatively large field of view of  $\sim 75$  mm. A laser light sheet is placed across the path of exhaust particles from a patient and imaged with a standard tablet camera. Side-scattered light eliminates the interference issues related to other techniques such as diverting the particle flow through a pipe.

A correlation and calibration method is presented whereby controlled particle sizes were generated using a range of simple spray nozzles and measured with a shadow imaging system. The shadow imaging system was able to capture the small (down to 20  $\mu\text{m}$ ) and fast (up to 10 m/s) particles with a high-speed camera at 10,000 fps and exposure time of 23  $\mu\text{s}$ , resulting in a field of view of 7.9 x 7.1 mm. The scaled/calibrated particle diameters were determined directly from their shadows. The same particle generators were then measured using the OR System which employs laser side-scatter imaging and a correlation is made to map the calibrated diameters from the shadow imaging system.

An aluminum frame and foam-board enclosure were constructed to position and align the system components while safely containing the laser light. The mobile OR System was developed for use in a hospital environment and the configuration was aligned with the needs of measuring airborne bodily exhaust during AGPs such as thoracotomies/thoracostomies and tracheotomies. To meet these requirements, the system was designed to be symmetric and reversible in order for the measurement aperture to be placed in proper proximity to the patient's body.

## Acknowledgments

This material is based upon research supported by, or in part by, a grant from Wake Forest School of Medicine and the U. S. Office of Naval Research under award number N00014-18-1-2754.

## References

1. Baron P. Generation and Behavior of Airborne Particles (Aerosols); (accessed August 2020). Available from: [https://www.cdc.gov/niosh/topics/aerosols/pdfs/aerosol\\_101.pdf](https://www.cdc.gov/niosh/topics/aerosols/pdfs/aerosol_101.pdf).
2. University Corporation for Atmospheric Research, 2007; 2007. Available from: <https://scied.ucar.edu/aerosols>.
3. Marr LC, Tang JW, Van Mullekom J, Lakdawala SS. Mechanistic insights into the effect of humidity on airborne influenza virus survival, transmission and incidence. *Journal of the Royal Society Interface*. 2019;16(150):20180298.
4. Asadi S, Wexler AS, Cappa CD, Barreda S, Bouvier NM, Ristenpart WD. Aerosol emission and superemission during human speech increase with voice loudness. *Scientific reports*. 2019;9(1):1–10.
5. Chao CYH, Wan MP, Morawska L, Johnson GR, Ristovski Z, Hargreaves M, et al. Characterization of expiration air jets and droplet size distributions immediately at the mouth opening. *Journal of Aerosol Science*. 2009;40(2):122–133.
6. Duguid J. The size and the duration of air-carriage of respiratory droplets and droplet-nuclei. *Epidemiology & Infection*. 1946;44(6):471–479.

7. Anfinrud P, Stadnytskyi V, Bax CE, Bax A. Visualizing speech-generated oral fluid droplets with laser light scattering. *New England Journal of Medicine*. 2020;.
8. Organization WH, et al. Joint ILO/WHO guidelines on health services and HIV/AIDS. In: *Joint ILO/WHO guidelines on health services and HIV/Aids*; 2005. p. 79–79.
9. Redlake MotionXtra HG-XL Imaging System; (accessed August 2020). Available from: <https://www.delimaging.com/camera/redlake-motionxtra-hg-xl-imaging-system/>.
10. Aerosol; (accessed August 2020). Available from: <https://en.m.wikipedia.org/wiki/Aerosol>.
11. Kulkarni P, Baron PA, Willeke K. *Aerosol measurement: principles, techniques, and applications*. John Wiley & Sons; 2011.
12. V3528-MPY 1.1” 35mm F2.8 12 Megapixel (C Mount) Lens; (accessed August 2020). Available from: <https://computar.com/product/1397/V3528-MPY>.
13. ARRI EB400/575D High Speed Ballast; (accessed August 2020). Available from: <https://www.arri.com/en/lighting/ballasts/discontinued>.
14. Arrilux 400 Lamp; 2020 (accessed August 2020). Available from: <https://www.arri.com/en/lighting/daylight/discontinued/arrilux>.
15. 610N-6 Spring-Tempered Steel Rules with Inch Graduations; 2020 (accessed August 2020). Available from: <https://www.starrett.com/metrology/product-detail/610N-6>.
16. Motion Studio 64bit; 2020 (accessed August 2020). Available from: <https://idtvision.com/products/software/motion-studio/>.
17. RayPower 5000, 5000mW 532Nm continuous laser; 2020 (accessed August 2020). Available from: <https://www.directindustry.com/prod/dantec-dynamics-s/product-15753-1842419.html>.
18. iPad Pro 11 specifications; 2020 (accessed August 2020). Available from: <https://www.apple.com/ipad-pro/specs/>.